Article

The lateralized LC-NAergic system distinguishes vicarious versus direct fear in mice

Jong-Hyun Kim[1], Da-Eun Choi [1] & Hee-Sup Shin [1,2] ✉

Fear can be induced either directly through self-experience of aversive events or vicariously by observing conspecifics experiencing such events. The locus coeruleus-norepinephrine (LC-NA) system is crucial in fear responses and cognitive processes. We investigated whether the LC-NA system differentially processes these two types of fear, direct and vicarious in male mice. The results highlighted that the right hemisphere LC→anterior cingulate cortex pathway is uniquely crucial for vicarious fear, while the two inputs to the LC− from the bed nucleus of the stria terminalis (BNST) and the central amygdala (CeA)−differentially contribute to fear processing. The BNST plays a more targeted role in vicarious fear, and the CeA has a broader influence on fear in general. This underscores the complexity and specialization within the LC-NA system for fear-processing.

Fear is a fundamental emotional response that can be triggered by direct experiences of aversive events or through social observation of others experiencing such events[1,2]. Direct fear arises from personal encounters with danger, while vicarious fear occurs when an individual witnesses conspecifics in distress. Both humans and animals possess the ability to acquire fear vicariously by observing conspecifics subjected to aversive events, a phenomenon termed observational fear (OF). OF, the empathic ability to vicariously experience another's aversive or fear events[3,4], plays a key role in fostering prosocial behavior[5,6]. Rodent studies have established behavioral models of OF as vicarious fear[7–9], and the ACC is a key region in the OF response[7,10–15].

One of the critical inputs to the ACC is the LC, which comprises a bilateral pair of nuclei located in the pons and serves as the primary supplier of norepinephrine (NA) to the brain. The NA is a major neuromodulator, exerting widespread effects throughout the central nervous system, and plays crucial roles in regulating various cognitive processes, including visual attention, arousal, and memory[16–22]. Moreover, several studies reveal that the LC-NA system is essential for direct fear responses, potentially through projections to the amygdala[23–25]. Despite extensive research into the LC-NA neural mechanisms underlying fear, the possibility for differential processing of fear responses, including vicarious vs direct fear, in this brain region remains largely unexplored. In this study, we investigated the unique function of the LC-NA system in regulating fear. The results highlighted the lateralization of the LC-NAergic system in these processes, revealing that the right hemisphere LC→ACC pathway is specifically crucial for vicarious fear. Meanwhile, the bed nucleus of the stria terminalis (BNST) and the central amygdala (CeA) inputs to the LC differentially contribute to fear processing. These findings underscore the complexity and specialization in processing of two types of fear within the context of emotion and social behavior, providing avenues for exploring empathy-related dysfunctions in psychiatric disorders.

Results

The functionally lateralized LC-NAergic system projecting to the ACC is involved in vicarious fear

The LC consists of a bilateral pair of nuclei located in the brainstem, with projections showing ipsilateral predominance[26,27]. To verify whether LC-NAergic neurons in each hemisphere project ipsilaterally to the corresponding side of the ACC, retrograde AAVs expressing mCherry or EGFP in a Cre-dependent manner (retroAAV-DIO-mCherry or retroAAV-DIO-EGFP) were simultaneously injected into the left-ACC (lACC) and right-ACC (rACC), respectively, in TH^Cre/+ mice (Supplementary Fig. 1a). Fluorescent signals were observed in the hemisphere injected with the virus, and these signals were rarely detected in the contralateral LC (Supplementary Fig. 1b, c). These results indicate that

[1]Center for Cognition and Sociality, Institute for Basic Science (IBS), 55 Expo-ro, Yusung-gu, Daejeon 34126, Republic of Korea. [2]IBS School, University of Science and Technology, Daejeon 34141, Korea. ✉e-mail: shin@ibs.re.kr

LC-NAergic neurons in each hemisphere predominantly project ipsilaterally to their corresponding sides of the ACC.

Previous studies involving naive observers have suggested the specific involvement of the right-side ACC in immediate, socially transmitted fear, demonstrating its necessity solely for vicarious fear responses[7,14]. Based on this, we examined the role of LC → ACC projections in the OF response by optogenetically inhibiting the LC terminals at the ACC in each hemisphere. To achieve this, we delivered AAVs expressing halorhodopsin (NpHR) or EYFP in a Cre-dependent manner (AAV-DIO-NpHR-YFP or AAV-DIO-YFP) into either the left LC (lLC) or right LC (rLC) in TH[Cre/+] mice. We then positioned optical fibers over the ACC to selectively inhibit inputs from each hemispheric LC during OF assays (Fig. 1a, b, f). Optogenetic inhibition of the rLC→rACC circuit resulted in decreased freezing behavior during OF assays compared to the control group (Fig. 1b, c). Interestingly, blocking the rLC→rACC circuit affects the maintenance of the freezing response but not the initiation of freezing behavior during OF. To validate this effect, we conducted temporal modulation to suppress the rLC→rACC pathway in ON-OFF states. The OF response was significantly reduced during photostimulation (Fig. 1d, e) and fully recovered to a control level when the laser was turned off (Fig. 1e). In contrast, inhibition of the lLC→lACC circuit did not affect freezing compared to the control group (Fig. 1f, g). These results reveal that the LC-NA system is involved in the OF response by maintaining freezing behavior and this function is lateralized to the right hemisphere.

Previous work showed that neuronal excitability in the ACC is enhanced by distinct adrenergic receptor (AR) subtypes, α1-adrenergic receptor (α1-AR) and β-adrenergic receptor (β-AR)[28]. To define the AR receptor types in the ACC involved in OF responses, we administered propranolol or prazosin, which are β-AR or α1-AR receptor antagonists respectively, through a cannula into either the lACC or rACC in observer mice, 15 min before OF assays (Fig. 1h). The administration of propranolol into the rACC significantly decreased freezing levels compared to the vehicle group (Fig. 1i, j). However, the infusion of propranolol into the lACC did not affect the OF freezing response (Fig. 1k, l). The infusion of prazosin into either the rACC or lACC did not alter the freezing response compared to the vehicle group (Supplementary Fig. 2a, b). These results suggest that the β-AR mediates the lateralized role of the LC → ACC projections in the OF response. Given the importance of visual sensory stimuli in the observational fear response[7,13,29], we investigated whether the LC → ACC circuit is also involved in another visual sensory dependent behavior assay, the looming-shadow test. In this behavior paradigm innate fear responses are directly triggered by overhead visual threats such as looming objects or predator silhouettes (Fig. 2a). Optogenetic silencing of either the rLC→rACC or lLC→lACC pathways did not impact freezing responses to the looming dark disk stimulus (Fig. 2b, c), implying that the LC → ACC circuit is not involved in visual-dependent, innate, direct fear. The LC-NA system is known to be pivotal in fear acquisition during the classical fear conditioning (CFC) test[25,30]. To explore the potential involvement of the LC → ACC projections in direct fear, we optogenetically inhibited these circuits in each hemisphere during classical fear conditioning (Fig. 2d). Inhibiting the LC → ACC projections, either right or left, did not influence freezing responses during fear conditioning or its subsequent memory tests (Fig. 2e, f). In conclusion, the right hemisphere-lateralized LC-NA projections to the ACC exclusively contribute to vicarious fear in OF responses via the β-AR.

The activity of ACC-projecting LC neurons in the right hemisphere is enhanced in vicarious fear, but not in direct fear

To examine the temporal dynamics of ACC-projecting LC neuronal activities during OF response, we unilaterally injected an AAV expressing GCaMP7fs in a Cre-dependent manner (AAV-FLEX-GCaMP7f) into the lLC or rLC of TH[Cre/+] mice. Subsequently, an optic fiber was implanted over the ACC on the corresponding hemisphere. Three

weeks later, we monitored calcium signal, which serves as an indicator of neuronal activity, at the LC noradrenergic axon terminals in each hemisphere of the ACC during OF assays, and then during the looming behavior test (Fig. 3a, b). During OF assays the calcium activity of the rLC→rACC projections gradually increased over the baseline beginning from 1 min after starting the foot-shock delivery to the demonstrator (Fig. 3c, e, Supplementary Fig. 3a).

In order to explore a possibility whether the LC neuron activity was temporally coupled to the foot shocks delivered to the demonstrator, the increase in LC-ACC GCaMP activity was compared between 2 s before and after the foot shock events. There were no significant changes in the neural activities between the two time points before and after the foot shock (Supplementary Fig. 3b). These results suggest that the activation of the LC neurons is not in direct responses to the foot-shocks delivered to the demonstrators.

To further investigate the activity of ACC neurons receiving inputs from the LC, we injected an anterograde trans-synaptic virus (AAV2/1-hsyn-Cre) into the LC and AAV-DIO-GCaMP into the ACC to monitor ACC neuronal responses during OF (Supplementary Fig. 4a, b). In alignment with the gradual increase in the LC axonal activity observed during OF training, ACC neuronal activities also exhibited a gradual increase (Supplementary Fig. 4c, d). Since the LC-NAergic fibers are known to form synaptic connections selectively with pyramidal neurons, rather than interneurons, in the ACC[28], these results suggest that ACC pyramidal neurons mediate the OF response. Meanwhile, no change was observed in the neuronal activity during the looming behavior test (Fig. 3f, h). Furthermore, no calcium signal changes were detected in the lLC→lACC circuit during either OF assays (Fig. 3d, e) or the looming test (Fig. 3g, h). These findings suggest that the LC-NA projections to the ACC are specifically involved in sustaining vicarious fear responses, and this function is lateralized to the right hemisphere.

The ACC-projecting LC neurons primarily receive inputs from the BNST and CeA

To analyze the specific presynaptic inputs of the ACC-projecting LC neurons responsible for the OF response, we conducted cTRIO (cell-type-specific Tracing of the Relationship between Input and Output) projection-specific input/output mapping in the right hemisphere. The cTRIO technologies enable the identification of monosynaptic inputs to specific starter cell types projecting to a selected output region[31–33]. Thus, this method provides precise and reliable results on the monosynaptic inputs to LC neurons projecting to the ACC. Initially, we injected a Cre-dependent retroAAV vector carrying the Flippase (Flp) recombinase (retroAAV-DIO-FLP) into the ACC of TH[Cre/+] mice. Subsequently, Flp- or Cre-activatable AAV vectors, AAV-Ef1α-FLEX fDIO-TVA-GFP and AAV-Ef1α-DIO-oRVG, were injected into the LC to express TVA and rabies glycoprotein, respectively. After 3 weeks, RV-ENVA-ΔG-DsRed was administered into the same site (i.e., LC) to label upstream neurons that establish direct synaptic contact with ACC-projecting LC neurons (Fig. 4a, b). Results revealed a wide range of upstream regions of the ACC-projecting LC neurons throughout the whole brain, including major inputs from fear/anxiety-related regions such as the BNST and the CeA (Fig. 4c, d). To further investigate the active roles of the BNST and CeA in the OF response, we repeated the cTRIO assay, combining it with c-Fos immunostaining—a marker for neuronal activity—in the BNST and CeA (Fig. 4e). Retrogradely labeled neurons in the BNST and CeA expressed c-Fos (Fig. 4f–h), indicating that both the BNST and CeA are involved in the OF response.

The BNST → LC → ACC but not the CeA→LC → ACC projections are specifically required for vicarious fear response

To verify the involvement of the BNST or CeA input to the LC → ACC pathway in regulating the OF response, we manipulated the targeting of axon terminals from the BNST or the CeA to the ACC-projecting LC neurons. First, we investigated whether inhibiting the BNST input to the
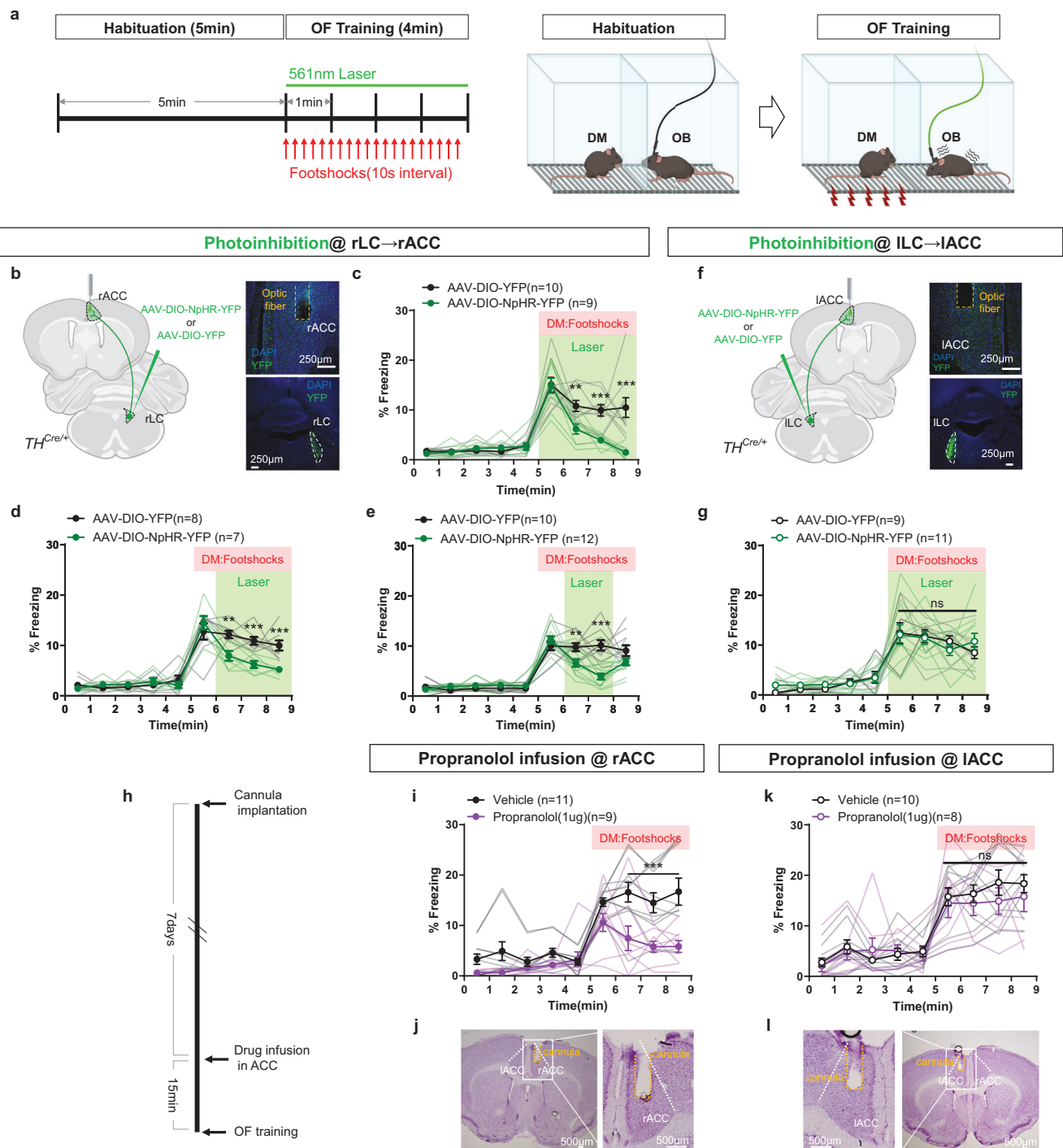
Fig. 1 | The LC-NA system in the right hemisphere is involved in the maintenance of vicarious fear of the OF response through β-AR in the rACC. **a** Diagram illustrating the observational fear behavioral paradigm with optogenetic manipulation. The observer (OB) and demonstrator (DM) mice are individually placed in the chamber and allowed to explore for 5 min (habituation). The observer mouse then watches the DM mouse receive foot shocks through a transparent partition for 4 min, while laser stimulation is applied to the OB mice for optogenetic manipulation. This figure was created using BioRender.com (https://BioRender.com/n96j318). **b**, **f** Schematic diagrams illustrating optogenetic inhibition of LC-NAergic neuronal axon terminals in the right-ACC (rACC) (**b**) or the left-ACC (lACC) (**f**). **c**, **g** Observational fear response in mice with continuous optogenetic suppression of LC-NAergic inputs in the rACC (**c**) (YFP $n = 10$, NpHR $n = 9$, Group (F (1, 17) = 32.71, $p < 0.0001$)) or lACC (**g**) (YFP $n = 9$, NpHR $n = 11$, Group

(F (1, 162) = 0.3307, $p = 0.5660$)). **d**, **e** Observational fear response in mice with laser ON-OFF modulation of LC-NAergic inputs in the rACC (**d**:YFP $n = 8$, NpHR $n = 7$, Group (F (1, 13) = 11.02, $p = 0.0055$), **e**:YFP $n = 10$, NpHR n = 12, Group (F (1, 20) = 15.32, $p = 0.0009$)). **h** Schematic of the drug infusion experimental procedures. **i**, **j** The effect of Propranolol in the rACC during OF training (**i**) (Vehcle $n = 11$, Propranolol $n = 9$, Group (F (1, 20) = 3.448, $p = 0.044$)) and the cannula position was verified by Nissl staining (**j**). **k**, **l** The effect of Propranolol in the lACC during OF training (**k**) (Vehcle $n = 10$, Propranolol $n = 8$, Group (F (1, 16) = 0.3569, $p = 0.5586$)) and confirmation of the cannula position (**l**). Data are presented as mean ± S.E.M. Error bars represent S.E.M. ns: not significant; *$p < 0.05$, **$p < 0.01$, ***$p < 0.001$ (two-way ANOVA followed by Sidak's multiple comparisons test for (**c**–**e**, **g**, **i**, **k**)). The exact p-values and source data are provided in the Supplementary Tables for statistical details and in the Source Data file.
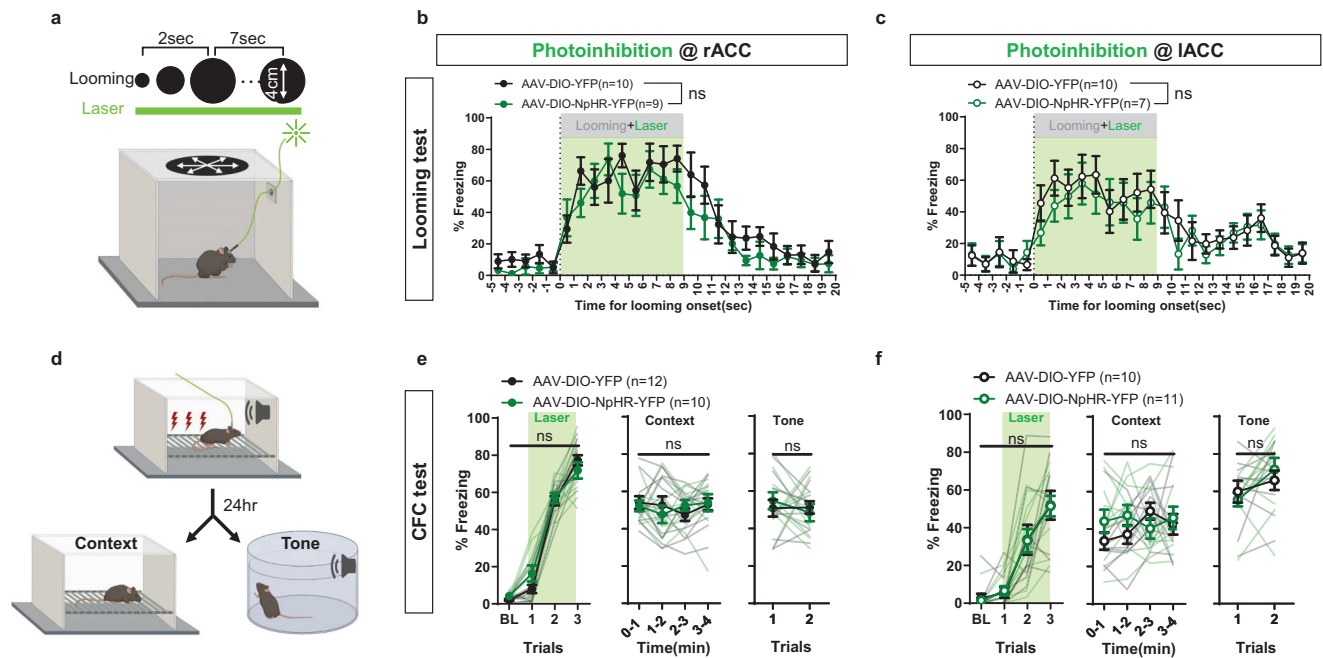
Fig. 2 | LC-NA inputs to the ACC are not involved in direct fear of the looming or CFC tests. a Schematic diagram illustrating optogenetic inhibition during the looming test. This figure was created using BioRender.com (https://BioRender.com/j61j226). **b**, **c** Quantification of freezing behavior with optogenetic inhibition in the rACC (**b**) (YFP $n = 10$, NpHR $n = 9$, Group (F $(1, 17) = 1.904$, $p = 0.1855$)) or the lACC (**c**) (YFP $n = 10$, NpHR $n = 7$, Group (F $(1, 19) = 0.3236$, $p = 0.5761$)) during the looming test. **d** Schematic diagram illustrating optogenetic inhibition during the CFC test. **e**, **f** Quantification of freezing behavior with optogenetic inhibition in the rACC (**e**) (YFP $n = 12$, NpHR $n = 10$, CFC conditioning: Group (F $(1, 20) = 0.4989$,

$p = 0.4881$), Context memory: Group (F $(1, 20) = 0.003333$, $p = 0.9545$), Cue memory: Group (F $(1, 20) = 0.02339$, $p = 0.8800$)) or the lACC (**f**) (YFP $n = 10$, NpHR $n = 11$, CFC conditioning: Group (F $(1, 19) = 0.002905$, $p = 0.9576$), Context memory: Group (F $(1, 19) = 0.4022$, $p = 0.5335$), Cue memory: Group (F $(1, 19) = 0.01338$, $p = 0.9091$)) during fear conditioning and its memory test after 24 h. Data are presented as mean ± S.E.M. Error bars represent S.E.M. ns: not significant; *$p < 0.05$, **$p < 0.01$, ***$p < 0.001$ (two-way ANOVA followed by Sidak's multiple comparisons test for (**b**, **c**, **e**, **f**)). The exact p-values and source data are provided in the Supplementary Tables for statistical details and in the Source Data file.

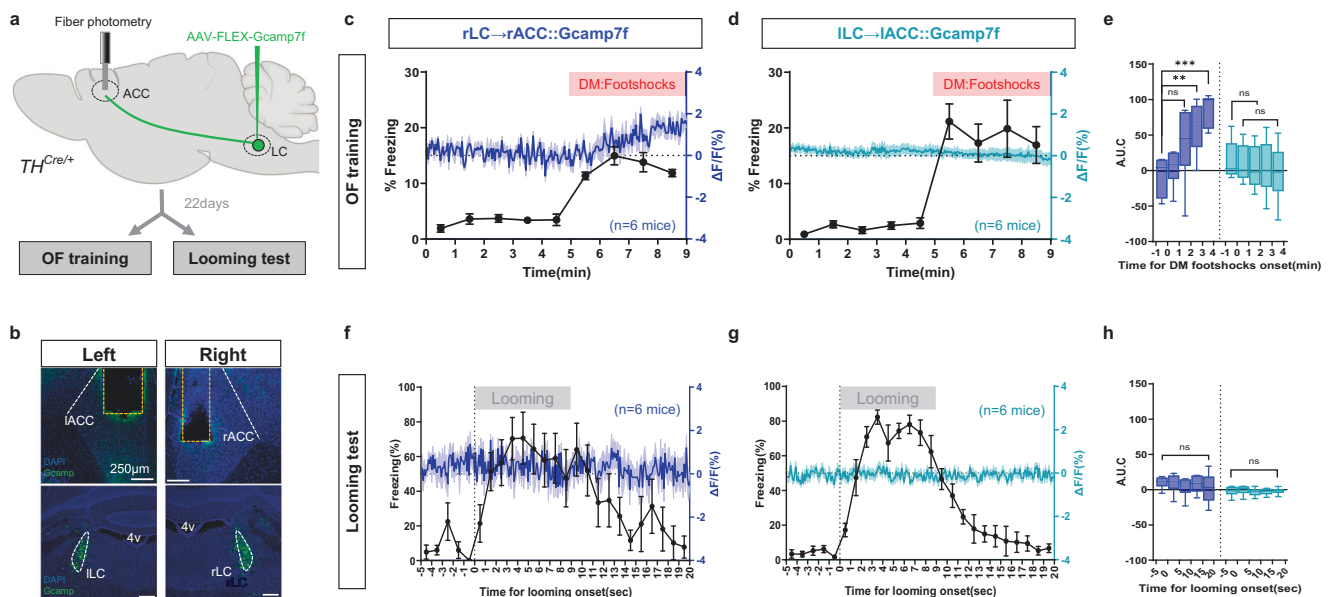**Fig. 3 | The activity of the rLC→rACC circuit is increased during vicarious fear of the OF response, but not during direct fear of the looming test. a** Schematic representation of the experimental process. This figure was created using BioRender.com (https://BioRender.com/d15f505). **b** Representative images showing the optic fiber position (orange dotted line) in the ACC and GCamp7f-expressing LC neurons in each hemisphere. **c–g** Recording of noradrenergic LC neuron axonal calcium signals in each hemisphere of the ACC during the OF training (**c**, **d**) or the looming test (**f**, **g**). (**c**, **d**, **f**, **g**: $n = 6$ mice: biological replicates, each derived from an

individual mouse). **e**, **h** Quantification of the area under the curve (AUC) of fluorescence changes in the OF training (**e**, left: F $(4, 25) = 7.325$, $p = 0.0005$, right: F $(8, 45) = 0.2816$, $p = 0.9687$) and the looming test (**h**, left: F $(4, 20) = 0.7968$, $p = 0.5413$, right: F $(4, 20) = 0.7183$, $p = 0.5894$). Data are presented as mean ± S.E.M. Error bars represent S.E.M. ns: ot significant; *$p < 0.05$, **$p < 0.01$, ***$p < 0.001$ (one-way ANOVA test for (**e**, **h**)). The exact p-values and source data are provided in the Supplementary Tables for statistical details and in the Source Data file.
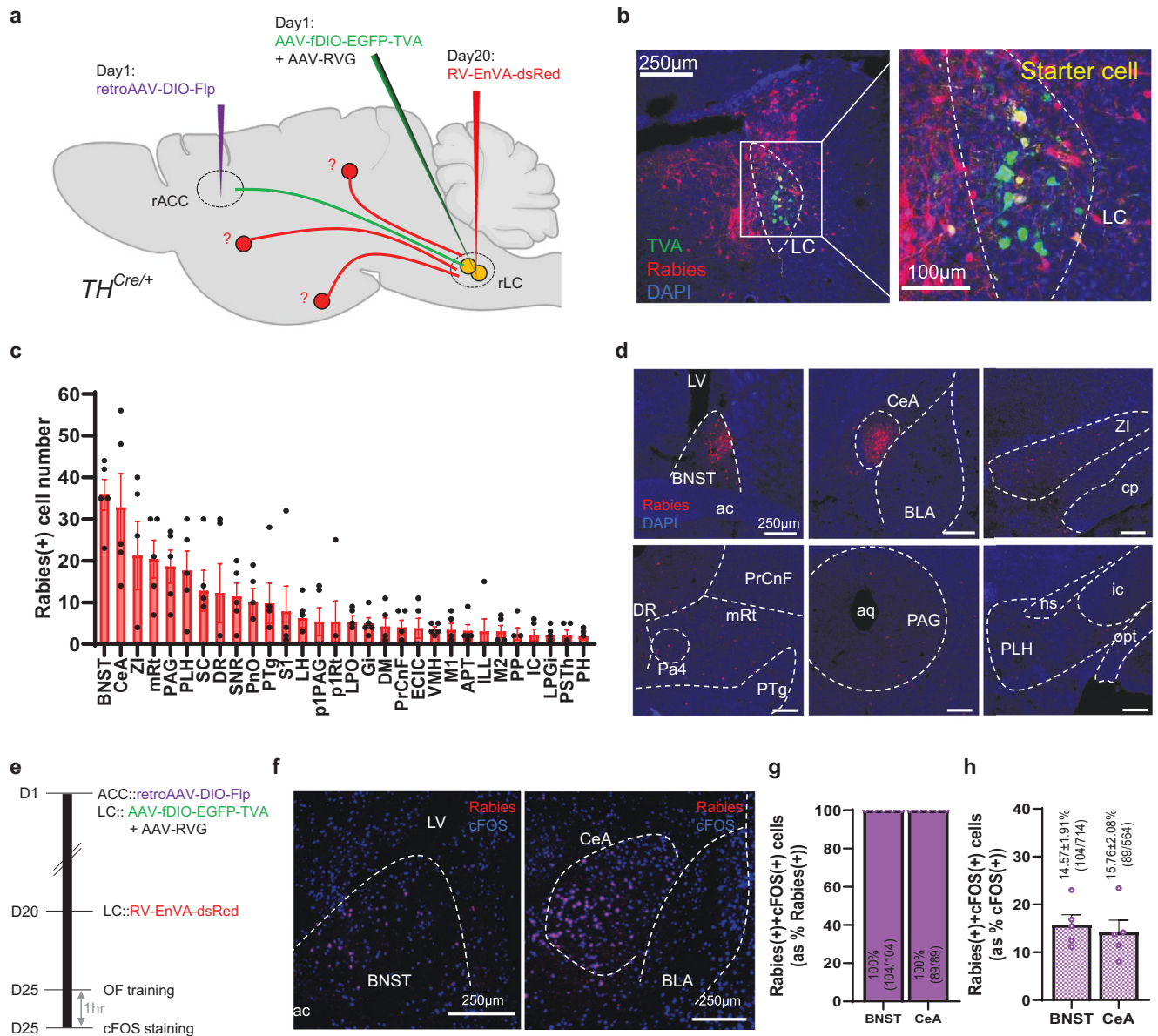
Fig. 4 | Monosynaptic afferents onto the LC→ACC circuits in the right hemisphere identified with a rabies virus-based, retrograde tracing system.
a Schematic of monosynaptic retrograde tracing from the ACC-projecting LC neurons. This figure was created using BioRender.com (https://BioRender.com/r34a603). **b** Starter neurons (yellow) in the LC. **c** Quantification of the presynaptic inputs (BNST Bed nucleus of the stria terminalis, CeA central amygdala, ZI zona incerta, mRT mesencephalic reticular, PAG periaqueductal gray, PLH peduncular part of lateral hypothalamus, SC superior colliculus, DR dorsal raphe, SNR substantia nigra, PnO oral part of pontine reticular nucleus, PTg pedunculotegmental nucleus, S1 primary somatosensory cortex, LH lateral hypothalamic area, LPO lateral preoptic area, Gi gigantocellular reticular nucleus, DM dorsomedial hypothalamic nucleus, PrCnF precuneiform area, SpVe spinal vestibular nucleus, ECIC external cortex of the inferior colliculus, VMH ventromedial hypothalamic nucleus, APT anterior pretectal nucleus, ILL intermediate nucleus of the lateral lemniscus,

M2 secondary motor cortex, PP peripeduncular nucleus, IC inferior colliculus, LPGi lateral paragigantocellular nucleus, PH posterior hypothalamic nucleus) ($n = 5$ mice: biological replicates, each derived from an individual mouse).
d Representative images of the top six upstream areas. The experiment was independently repeated 5 times with similar results. **e** Schematic diagram illustrating the experimental timeline for c-Fos immunostaining combined with cTRIO retrograde labeling ($n = 5$ mice: biological replicates, each derived from an individual mouse). **f** Representative images showing the colocalization of retrograde-labeled neurons (Rabies-positive, red) and c-Fos-positive neurons (blue) in the BNST and CeA. The experiment was independently repeated 5 times with similar results.
g, **h** Quantification of the percentage of Rabies-positive neurons coexpressing c-Fos in the BNST and CeA. Data are presented as mean ± S.E.M. Source data corresponding to this figure are reported in the Source Data file.

LC → ACC circuit affects the OF response (Fig. 5a). First, we injected retroAAV-DIO-FlpO into the ACC to induce Flp-recombinase expression in LC-NAergic neurons projecting to the ACC in TH$^{Cre/+}$ mice. Subsequently, we administered a Flp-dependent AAV expressing WGA-Cre into the LC, and an AAV-DIO-NpHR into the BNST. This approach led to the expression of NpHR in the BNST neurons, labeled with the retrograde Cre recombinase derived from the ACC-projecting LC neurons. Concurrently, an optic fiber was implanted into the LC of these mice

(Fig. 5a, Supplementary Fig. 5a, b). Photostimulation of NpHR-expressing BNST neuron terminals in the LC reduced the maintenance of freezing response during OF assays compared to the control group (Fig. 5b). On the other hand, this optogenetic modulation did not affect the looming or CFC tests (Fig. 5c, d), consistent with the results described above with the LC → ACC projections. Next, we investigated the requirement of CeA inputs to the LC → ACC circuits in the OF response, following a procedure similar to that used for the optogenetic
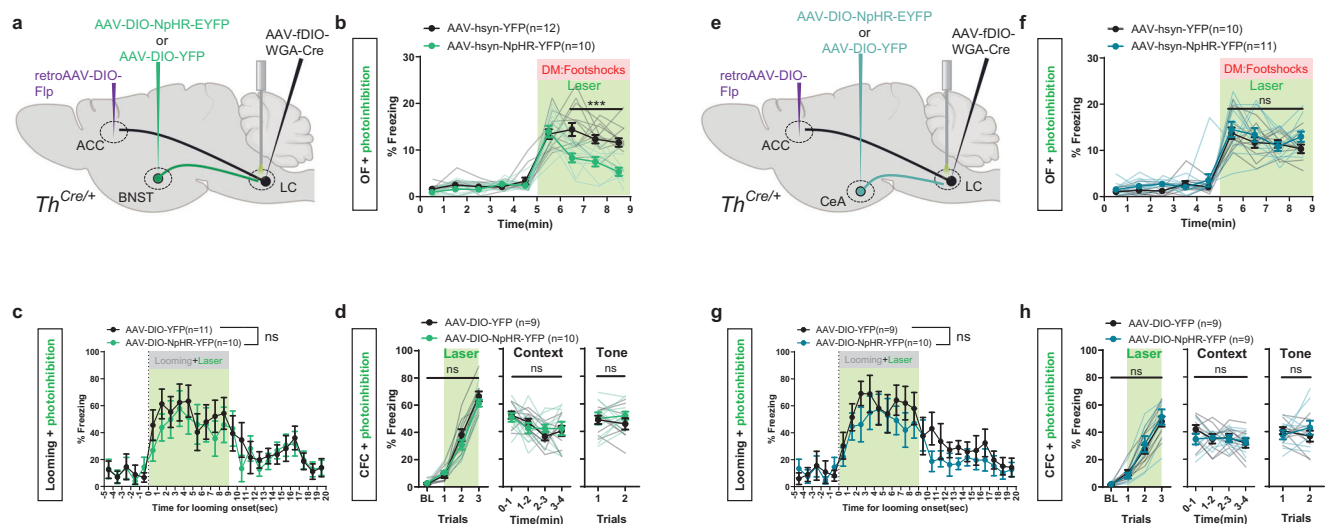
Fig. 5 | Optogenetic inhibition of the selective BNST inputs onto the LC→ACC circuit decreases various fear of the OF response, but not direct fear. Selective CeA inputs onto the LC→ACC circuit have no effect on fear in general. a, e Schematic of Cre- and Flp-dependent optogenetic inhibition for the BNST inputs (**a**) and central amygdala (CeA) inputs (**e**) in the LC→ACC circuit. This figure was created using BioRender.com (https://BioRender.com/o12y210). **b, f** Freezing response with optogenetic inhibition of the BNST inputs (**b**) (YFP $n = 12$, NpHR $n = 10$, Group (F (1, 20) = 24.17, $p < 0.0001$)) and CeA inputs (**f**) (YFP $n = 10$, NpHR $n = 11$, Group (F (1, 19) = 2.597, $p = 0.1236$)) onto the LC→ACC pathway during OF training. **c, g** Level of freezing behavior with photoinhibition of BNST inputs (**c**) (YFP n = 11, NpHR $n = 10$, Group (F (1,19) = 0.3236, $p = 0.5761$)) and CeA inputs (**g**) (YFP $n = 9$, NpHR $n = 10$, Group (F (1, 17) = 1.222, $p = 0.9794$)) to the LC→ACC circuit

during the looming test. **d, h** Level of freezing behavior with optogenetic inhibition of BNST inputs (**d**) (YFP $n = 9$, NpHR $n = 10$, CFC conditioning: Group (F (1, 17) = 1.223, $p = 0.2842$), Context memory: Group (F (1, 68) = 0.02767, $p = 0.8684$), Cue memory: Group Group (F (1, 17) = 0.6865, $p = 0.4189$)) and CeA inputs (**h**) (YFP $n = 9$, NpHR $n = 9$, CFC conditioning: Group (F (1, 15) = 0.1274, $p = 0.7261$), Context memory: Group (F (1, 16) = 0.2998, $p = 0.5916$), Cue memory: Group (F (1, 16) = 0.1439, $p = 0.7094$)) onto the LC→ACC pathway during the CFC test. Data are presented as mean ± S.E.M. Error bars represent S.E.M. ns: not significant; *$p < 0.05$, **$p < 0.01$, ***$p < 0.001$ (two-way ANOVA followed by Sidak's multiple comparisons test for (**b**–**d**), and (**f**–**h**)). The exact p-values and source data are provided in the Supplementary Tables for statistical details and in the Source Data file.

experiments conducted on the BNST (Fig. 5e, Supplementary Fig. 5c, d). In contrast to the results with the BNST, optogenetic modulation of CeA inputs to the LC→ACC circuit did not impact fear response in OF (Fig. 5f). Interestingly, it did not influence other fear responses as in the looming, and CFC tests (Fig. 5g, h). These results indicate that the BNST→LC→ACC pathway, rather than the CeA→LC→ACC circuit, plays a critical role in regulating the vicarious fear response.

The BNST's role is specific to vicarious fear and the CeA is required for fear in general

To expand our understanding of the engagement of the BNST and CeA in various fear responses, we employed a nonselective optogenetic inhibition approach to target the input to the LC from the BNST or CeA. We non-selectively expressed NpHR or YFP (AAV-hSyn-NpHR-YFP or AAV-hsyn-YFP) in the BNST or the CeA neurons and subsequently placed an optic fiber into the LC (Fig. 6a, e, Supplementary Fig. 6a–d). Nonselective blockade of BNST inputs to the LC reduced the freezing behavior during the maintenance phase of OF assays compared to the control group, yet showed no impact on looming and CFC tests (Fig. 6b–d), results consistent with those of the BNST→LC→ACC circuit-selective modulation described above (Fig. 5b–d). Conversely, blocking the general input from the CeA to the LC completely abolished the freezing behavior in OF, including the initiation of freezing (Fig. 6f). Furthermore, this inhibition eliminated the freezing level in the looming test and suppressed fear acquisition in the CFC test (Fig. 6g, h). Overall, our findings suggest that the BNST is specifically involved in mediating vicarious fear, while the CeA is broadly involved in freezing behavior in general.

Inhibition of the LC→BLA projections recapitulates the results of the CeA→LC suppression

One particular efferent projection from the LC is to the basolateral amygdala (BLA)[34–36]. The BLA is notable for encoding and driving

affective behaviors, including anxiety and fear, by interacting with the LC-NA system[15,37–39]. These previous findings led us to hypothesize that the LC→BLA circuit could play a critical role in various fear responses.

First, to test whether the LC neurons collaterally project to both the ACC and BLA, we used retrograde AAVs expressing mCherry or EGFP in a Cre-dependent manner. These were simultaneously injected into the right BLA (rBLA) and right ACC (rACC), respectively, in TH^Cre/+ mice (Supplementary Fig. 7a, b). The results revealed that distinct neuronal populations in the LC project to the BLA or the ACC, respectively (Supplementary Fig. 7c, d). To investigate the involvement of the LC→BLA circuit in several fear responses, we injected a cre-dependent NpHR-expressing AAV into the LC of TH^Cre/+ mice and implanted an optic fiber into the BLA (Fig. 7a, Supplementary Fig. 8a, b). Then, LC inputs to the BLA was inhibited by photostimulation during OF, looming, and CFC tests. The inhibition of the LC→BLA circuit blocked freezing behavior during OF (Fig. 7b), looming (Fig. 7c), and CFC test (Fig. 7d), aligning with our findings from the CeA→LC circuit inhibition. These findings suggest that the CeA inputs to the LC→BLA circuit may contribute to fear responses in general.

To assess the connection between the CeA and the LC→BLA circuit, we repeated the cell type-specific rabies tracing (cTRIO) on the BLA-projecting LC neurons (Fig. 7e). We found that the CeA is the predominant upstream brain region to the LC→BLA circuit (Fig. 7f, g), suggesting that the CeA, as an upstream region, directly modulates the LC→BLA pathway involved in general fear responses.

Discussion

In this study, we elucidate the critical roles of the LC-NA system distinguishing vicarious from direct fear, and the distinct contributions of the BNST and CeA to fear responses. Our study yielded several key findings: (i) Functional lateralization of the LC projections to the ACC in mediating OF responses; (ii) The involvement of β-ARs in mediating the lateralized role of the LC→ACC pathway; (iii) Temporal dynamics
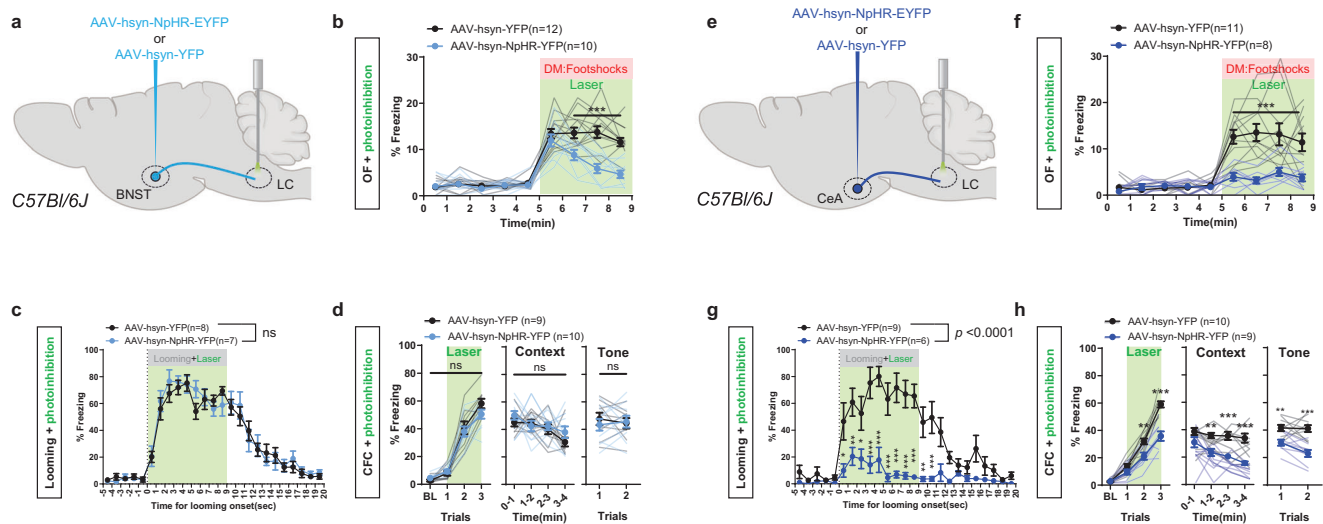
Fig. 6 | Inhibiting nonselective BNST inputs to the LC attenuates only the vicarious fear of the OF response, whereas inhibiting nonselective CeA inputs to the ACC suppress fear in general. a, e Schematic of nonselective optogenetic silencing for the BNST inputs (**a**) and CeA inputs (**e**) to the LC. This figure was created using BioRender.com (https://BioRender.com/s27c507). **b, f** Freezing response with optogenetic inhibition of the BNST inputs (**b**) (YFP $n = 12$, NpHR $n = 10$, Group (F (1, 20) = 30.98, $p < 0.0001$)) and CeA inputs (**f**) (YFP $n = 11$, NpHR $n = 8$, Group (F (1, 17) = 20.47, $p = 0.0003$)) to the LC during OF training. **c, g** Quantification of freezing levels with photoinhibition of BNST inputs (**c**) (YFP $n = 8$, NpHR $n = 7$, Group (F (1, 18) = 0.04483, $p = 0.8347$)) and CeA inputs (**g**) (YFP $n = 9$, NpHR $n = 6$, Group (F (1, 16) = 34.20, $p < 0.0001$)) to the LC during the looming test.

d, h Level of freezing behavior with optogenetic inhibition of BNST inputs (**d**) (YFP $n = 9$, NpHR $n = 10$, CFC conditioning: Group (F (1, 17) = 0.6408, $p = 0.4345$), Context memory: Group (F (1, 17) = 2.068, $p = 0.1685$), Cue memory: Group (F (1, 17) = 0.08895, $p = 0.7691$)) and CeA inputs (**h**) (YFP $n = 10$, NpHR $n = 9$, CFC conditioning: Group (F (1, 68) = 41.52, $p < 0.0001$), Context memory: Group (F (1, 17) = 31.65, $p < 0.0001$), Cue memory: Group (F (1, 34) = 35.92, $p < 0.0001$)) to the LC during the CFC test. Data are presented as mean ± S.E.M. Error bars represent S.E.M. ns: not significant; *$p < 0.05$, **$p < 0.01$, ***$p < 0.001$ (two-way ANOVA followed by Sidak's multiple comparisons test for (**b–d**) and (**f–h**)). The exact p-values and source data are provided in the Supplementary Tables for statistical details and in the Source Data file.

of ACC-projecting LC neuronal activity in the right hemisphere during OF responses; (iv) The differential roles of inputs from the BNST and CeA to the LC in regulating various fear responses. Collectively, these findings identify a unique, lateralized LC-NA system projecting to the ACC, which selectively mediates vicarious fear with inputs from the BNST.

Many studies have demonstrated that the LC-NA system enhances the brain's responsiveness to external stimuli by modulating cortical activity. This modulation plays a crucial role in maintaining sustained attention and facilitating the processing of relevant information while filtering out distractions[16,40]. The ACC is also involved in attentional processes, particularly in sustained attention tasks. It shows increased activity during the presentation of salient, distracting stimuli and during error processing−situations that demand shifts in attention or behavioral responses[41,42]. While the LC-hippocampal pathway demonstrates specific responses to direct footshock events during contextual fear conditioning[43], an intriguing aspect of our findings is that the LC → ACC projections exhibit a gradual and general increase in activity, which does not appear to be temporally coupled to the demonstrator's shock events. These findings highlight the role of the LC → ACC projections in maintaining, rather than initiating, freezing behavior during vicarious fear responses, highlighting the role of the LC → ACC in processing emotional and attentional components of fear. By projecting to the ACC, the LC-NAergic system may enhance the observer's focus on the distress signals exhibited by the demonstrator, rather than simply responding to the foot-shock events delivered to the demonstrator. This heightened attention could ensure that the observer remains vigilant and responsive to potential threats, facilitating adaptive social learning. This mechanism may be critical for the observer to continually update their behavioral response based on ongoing social information, highlighting the sophisticated interplay between the noradrenergic system and higher-order cognitive processes in social fear learning.

The LC-NA system modulates neural oscillations, particularly theta rhythms (4–8 Hz), across multiple brain regions such as the hippocampus, prefrontal cortex, and amygdala[44–47]. Theta oscillations are believed to temporally coordinate neural ensembles and facilitate communications across distributed networks. Theta rhythm, an oscillatory pattern in neural activity occurring at frequencies of ~4–8 Hz, i.e. Type-2 theta, has been linked to various cognitive processes, including memory, spatial navigation, and attention[18,48–52]. Additionally, theta oscillations have been observed in brain regions involved in fear processing and may serve as a mechanism for coordinating neural activity during fear-related behaviors[25,53]. Interestingly, our previous study showed that synchronized Type-2 theta oscillations in the reciprocal ACC-BLA circuits in the right hemisphere are coupled temporally and quantitatively with the freezing events driving the OF response[15]. The current findings suggest a possibility that the LC-noradrenergic system may regulate vicarious fear response via modulating theta oscillations within this cingulate-amygdala circuit.

The β-AR is a G protein-coupled receptor that is broadly expressed in neurons, microglia, and astrocytes in the brain[54,55]. Activation of β-ARs on pyramidal neurons is known to increase their excitability by modulating potassium channels and enhancing NMDA receptor currents[54,56]. Additionally, β-AR signaling can interact with L-type calcium channels (LTCCs)[57,58]. Activation of β-AR modulates LTCC activity through cAMP-dependent mechanisms, leading to changes in intracellular calcium levels and downstream cellular functions. Indeed, the impairment of LTCC in the ACC resulted in a loss of freezing behavior maintenance during OF assays[7], replicating the results observed with β-AR blocker infusion. These observations suggest a possibility that β-AR modulates ACC pyramidal neuronal excitability through LTCC, thereby contributing to the OF response.

It is interesting to see that the hemispheric lateralization of observational fear extends to the LC → ACC projections. Research on the function of the LC in pupil dilation regulation suggested that there
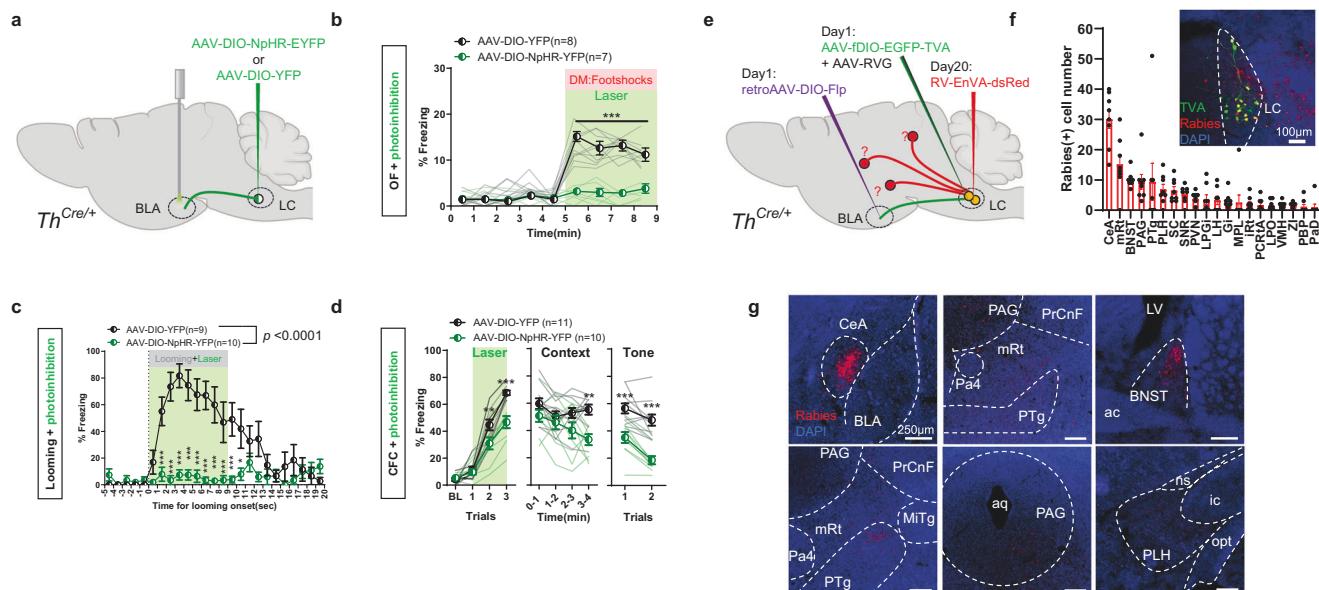
Fig. 7 | Inhibiting nonselective CeA inputs to the LC → BLA circuit suppress fear in general. a Schematic diagram depicting optogenetic suppression of the LC → BLA circuit in the right hemisphere. This figure was created using BioRender.com (https://BioRender.com/y27w009). **b–d** Levels of freezing behavior in mice with optogenetic suppression of the LC → BLA circuit during OF training (**b**) (YFP $n = 8$, NpHR $n = 7$, Group (F (1, 13) = 60.23, $p < 0.0001$)), looming test (**c**) (YFP $n = 9$, NpHR $n = 10$, Group (F (1, 18) = 89.32, $p < 0.0001$)), and CFC test (**d**) (YFP $n = 11$, NpHR $n = 10$, CFC conditioning: Group (F (1, 19) = 9.332, $p = 0.0065$), Context memory: Group (F (1, 76) = 15.70, $p = 0.0002$), Cue memory: Group (F (1, 19) = 28.80, $p < 0.0001$)). Data are presented as mean ± S.E.M. Error bars represent S.E.M. ns: not significant; *$p < 0.05$, **$p < 0.01$, ***$p < 0.001$ (two-way ANOVA followed by Sidak's multiple comparisons test for (**b–d**)). The exact p-values and source data are provided in the Supplementary Tables for statistical details and in the Source Data file. **e** Schematic of monosynaptic retrograde tracing from the BLA-projecting LC

neurons. This figure was created using BioRender.com (https://BioRender.com/y27w009). **f** Quantification of the presynaptic inputs ($n = 8$ mice) (CeA central amygdala, mRT mesencephalic reticular, BNST Bed nucleus of the stria terminalis, PAG, periaqueductal gray, PTg pedunculotegmental nucleus, SC superior colliculus, SNR substantia nigra, PVN paraventricular nucleus, LPGi lateral para-gigantocellular nucleus, LH lateral hypothalamic area, Gi gigantocellular reticular nucleus, MPL medial paralemniscal nucleus, iRt intermediate reticular nucleus, PCRtA alpha part of parvicellular reticular nucleus, PCRtA alpha part of parvicellular reticular nucleus, LPO lateral preoptic area, VMH ventromedial hypothalamic nucleus, ZI zona incerta). The right image shows starter neurons (yellow) in the LC. Source data corresponding to this figure are reported in the Source Data file. **g** Representative images of the top six upstream areas. The experiment was independently repeated 8 times with similar results.

might be lateralized effects[59]. Here, we found different intensities of LC neuronal activities in the projections to the ACC between the two hemispheres during the OF response. This effect may be due to functional and structural differences between the left and right LC. The right hemisphere plays a dominant role in processing certain negative emotions like fear, anxiety, and responses to stress, which could influence the activity of the LC-NA system in the right hemisphere[60,61]. Meanwhile, some studies have reported an asymmetry, with more neurons present in the right LC compared to the left[62]. These suggested that the differences in the strength or patterns of connectivity between the left and right LC may influence lateralized functions[63]. It is also conceivable that the right and left LC may differ in the ability to modulate theta oscillatory dynamics during observational fear. Yet another possibility exists that the input signals are already lateralized when arriving at the LC.

The BNST and CeA are part of the extended amygdala complex and play a crucial role in the expression of fear and anxiety-related behaviors[64–67]. These regions receive inputs from various sources, including sensory information and contextual cues associated with potential threats. While the BNST is a minor input to the LC (Fig. 7e–g), chronic stress or prolonged BNST activation can lead to sustained dysregulation of NA in the LC, which is associated with depression. For instance, chemogenetic activation of Vgat-expressing neurons in the BNST increases anxiety-like behavior and activates the LC[68]. In OF, the BNST may integrate emotional and sensory information about observed threats, such as visual cues indicating danger. Some fMRI studies have reported a significant increase in the BNST activity in response to visual threat stimuli of objects (such as a spider)[69,70]. Also, BNST mediates the sustained

(anxiety-like) fear responses to long-duration threats[71–73]. It is conceivable that the BNST processes socially transferred fear induced by continued visual threat stimuli and sends signals to downstream brain regions, including the LC → ACC pathway, to trigger vicarious fear. The CeA primarily functions as a central hub for processing fear-related stimuli and coordinating fear responses[71,74]. Specifically, by releasing the Corticotropin-Releasing Factor (CRF) in the CeA, descending CeA→LC projections amplify LC excitability, potentiate NAergic efferent effects on BLA principal cells, and drive feed-forward excitation of the BLA neuronal activity. This ultimately results in heightened sensitivity to threats and improved fear recognition[75]. Thus, our finding that silencing either the CeA→LC or LC → BLA circuit negates the fear response is consistent with their crucial contribution to fear processing in general.

Our manipulation of the CeA→LC → ACC circuit did not yield any effects on fear responses (Fig. 5), but some findings in the literature suggests that this pathway may have significant implications for sleep regulation. The LC-NAergic projections to the ACC could be involved in facilitating transitions between sleep stages[76,77], as evidenced by observed changes in ACC activity patterns during these transitions[78]. Additionally, the CeA's known influence on sleep onset and rapid eye movement (REM) sleep regulation[79] further supports the potential importance of this circuit in sleep processes. However, the precise mechanisms and extent of this circuit's involvement in sleep processes require further investigation.

While our study does not exclude potential involvements of other brain regions in differentially processing vicarious vs direct fear, it offers insights into the unique and specific LC-NAergic system in this brain functions. The differential engagement of these LC-NAergic

system highlights the complexity and specificity of fear processing in the brain.

Methods

Animals
Mice had free access to food and water and were maintained under a 12 h light/dark cycle at 20–26 °C with 40–60% humidity, with the light cycle beginning at 08:00 AM. All protocols for animal experiments were approved by the Institutional Animal Care and Use Committee (IACUC) of the Institute of Basic Science (Daejeon, Korea). The TH$^{Cre/+}$ (Strain #008601) and C57Bl/6J (Strain #000664) mouse lines were obtained from the Jackson laboratory. All mouse lines were backcrossed with C57BL/6J for >9 generations and only male mice were used in all studies.

Stereotaxic surgery
Mice were anesthetized by isoflurane gas anesthesia (induction at 3.5%, and maintenance at 1.5–2%, the Dräger Vapor® 2000; Draeger), and then placed on a stereotaxic frame (David Kopf Instruments). Holes were drilled with a micromotor handpiece drill (Foredom) after the exposure of the skull. Viruses were injected using a pulled fine-glass capillary (#GC150F-4/X, Warner Instruments) connected to a Microliter syringe (#84850, Hamilton) with Tygon tubing. The syringe was placed on an infusion pump (#70-2002, Harvard Apparatus) for a steady injection rate of 0.04 μL/min. Unilateral (on the left or right side) virus injections were made for the following target regions: LC (anteroposterior (AP), -5.4 mm; mediolateral (ML), 0.84 mm; dorsoventral (DV) -4.0 mm from bregma), ACC (AP, 1.1 mm; ML, ±0.3 mm; DV, -1.6 mm), BNST(AP, 0.15 mm; ML, 1.1 mm; DV, -4.2 mm), CeA (AP, -1.4 mm; ML, 2.9 mm; DV, -4.6 mm), and BLA(AP, -1.2 mm; ML, 3.2 mm; DV, -4.9 mm). A total volume of 0.4 μL of the virus was injected, and the fine-glass capillary was slowly removed from the injection site 8 min after injection.

For retrograde tracing of inputs to the LC neurons, 0.4 μL of retroAAV-DIO-mCherry-WPRE-hGHpA (5.71 × 10^{12}vg/ml^{-1}) and retroAAV-DIO-GFP-WPRE-hGHpA (5.13 × 10^{12}vg/mL) were simultaneously injected into the lACC and rACC. Mice were sacrificed 20-22 days after the injection.

For retrograde tracing of inputs to the LC neurons from the rACC and rBLA, 0.4 μL of retroAAV-DIO-mCherry-WPRE-hGHpA (5.71 × 10^{12}vg/ml^{-1}) and retroAAV-DIO-GFP-WPRE-hGHpA (5.13 × 10^{12}vg/mL) were simultaneously injected into the rACC and rBLA. Mice were sacrificed 20-22 days after the injection.

For monitoring the output of each hemispheric LC neuron via fiber photometry, 0.4 μL of AAV9-CAG-FLEX-GCamp7f-WPRE-SV40pA (5.23 × 10^{12}vg/mL) as injected unilaterally into the LC of TH$^{Cre/+}$ transgenic mice, and a black ceramic mono fiber-optic cannula (400 μm, 0.39NA, #R-FOC-BL400C-39NA, RWD) was implanted in the lACC or rACC.

For optogenetic axon terminal inhibition of LC neurons projecting to ACC, 0.4 μL of AAV5-hSyn-DIO-eNpHR3.0-EYFP-WPRE-hGHpA (4.53 × 10^{12}vg/mL) was injected unilaterally into each hemisphere of the LC in TH$^{Cre/+}$ mice. A ceramic monofiber-optic cannula (200 μm, 0.37 NA, Newdoon) was implanted in the corresponding ACC. Experiments took place 3 weeks after injection.

For monitoring the rACC neurons receiving inputs from the rLC neuron via fiber photometry, 0.4 μL of AAV2/1-hSyn-CRE (2.33 × 10^{12}vg/ml^{-1}) and AAV9-CAG-FLEX-GCamp7f-WPRE-SV40pA (5.23×10^{12}vg/mL) were simultaneously injected into the rLC and rACC, and a black ceramic mono fiber-optic cannula (400 μm, 0.39NA, #R-FOC-BL400C-39NA, RWD) was implanted in the rACC.

For the "cell-type-specific tracing of input-output" (CTRIO) tracing of the LC-NAergic neurons, retroAAV-EF1a-FLP-WPRE-hGHpA (0.4 μL, 2.5 × 10^{12}vg/mL) was injected into the rACC, and a combination of AAV9-EF1a-fDIO-EGFP-T2a-TVA-WPRE-hGHpA/

AAV9-EF1a-DIO-oRVG-WPRE-hGHpA (0.4 μL each, 2.53 × 10^{12}vg/mL) was injected into rLC. After 25 days, RV-Env-ΔG-dsRed (0.5 μL, 2 × 10^{8}vg/mL) was injected into LC. Five days later, mice were perfused and tracing was confirmed via histology.

For optogenetic axon terminal inhibition of the selective BNST or the CeA to ACC-projecting LC neurons, retroAAV-EF1a-FLP-WPRE-hGHpA (0.4 μL, 2.5 × 10^{12} vg/mL) was injected into the rACC, and 0.4 μL of AAV5-hSyn-fDIO-WGA-CRE-P2A-WPRE-hGH polyA (2.0 ×10^{12}vg/mL) was injected into the right hemisphere of the LC. Then, AAV5-hSyn-DIO-eNpHR3.0-EYFP-WPRE-hGHpA was injected into the BNST or the CeA in TH$^{Cre/+}$ mice. A ceramic monofiber-optic cannula (200 μm, 0.37 NA) was implanted in the LC. Behavioral experiments took place 6 weeks after injection.

For optogenetic axon terminal inhibition of the nonselective BNST or the CeA to LC neurons, AAV5-hSyn-eNpHR3.0-EYFP-WPRE-hGHpA (2.0 × 10^{12}vg/mL) was injected into the BNST or the CeA in naive mice. Subsequently, a ceramic monofiber-optic cannula (200 μm, 0.37 NA) was implanted in the LC.

For directly administrating or their respective vehicles into the ACC, mice were first anesthetized by intraperitoneal (i.p.) injection of ketamine/xylene (120 mg/kg). A cannula (PlasticsOne) was unilaterally implanted in the lACC or rACC (AP; +1.1 mm, ML; ±0.3 mm, and DV; -1.7 mm).

Drug preparation and infusion
Propranolol hydrochloride (0624, Tocris) and Prazosin hydrochloride (0623, Tocris) were dissolved in PBS containing 1% Dimethyl sulfoxide (DMSO). All the drugs were infused into each brain area via an inner cannula (33 gauge) connected to a 0.25 μl Hamilton syringe. The flow rate (0.25 μl/min) was regulated with a syringe pump (SP100i; WPI). Behavior experiments began 15 min after a single infusion.

Tissue processing and histology
Mice were anesthetized by i.p. injection of ketamine/xylazine (120 mg/kg) before transcardial perfusion with 100 ml of 0.1 M phosphate-buffered saline (PBS, pH 7.4), followed by transcranial perfusion with 50 ml of 4% paraformaldehyde in 0.1 M PBS (pH 7.4) at 4 °C per mouse. Brains were removed, followed by post-fixing for 24 h in the same fixative and cryoprotecting by immersing in 30% sucrose for 2 days. Coronal 45μm sections of the LC were washed and blocked with 0.1 M PBS containing 0.3% Triton X-100 plus 3% normal donkey serum (NDS). Slices were then incubated overnight at 4 °C with the designated primary antibodies, appropriately diluted in PBS. The following primary antibodies were used in this study: mouse monoclonal anti-TH (1:2000 dilution, MAB314, Sigma-Aldrich) and rabbit polyclonal c-Fos (1:3000 dilution, sysy226008, Synaptic Systems). After that, the slices were washed three times with PBS and then incubated for 2 h with Alexa 647-conjugated donkey anti-mouse IgG (1:1000 dilution, Jackson immunoresearch) and Alexa 647-conjugated donkey anti-rabbit IgG (1:1000 dilution, Jackson immunoresearch) secondary antibodies, as appropriate, diluted in 0.1 M PBS. Slices were then washed three times in PBS containing 0.3% Triton X-100, mounted on subbed slides, air dried, and coverslip-mounted using DAPI Fluoromount-G mounting medium containing DAPI (0100-20, Southernbiotech).

Fiber photometry
A TDT RZ5P fiber photometry system and Synapse software were used in this study. Briefly, light from the 470 nm, 17.2 mW (Min) fiber-coupled LED (Thorlabs) and light from the 405 nm, 19.3 mW (Min) fiber-coupled LED (Thorlabs) was directed into a fluorescence mini cube with six ports and a built-in detector head (Doric Lenses), with spectral bandwidths of 405 and 470 nm. A 405 nm light was modulated at 210 Hz, while 470 nm light was modulated at 330 Hz. For both wavelengths, power output was kept at 20 mA with a 3 mA DC offset. The light was then directed through a fiber-optic patch cord with a

400 μm core (Doric Lenses). This fiber was linked to the mono-fiberoptic cannulas implanted in the area of interest.

Optogenetic stimulations

The optogenetic stimulation procedure involved the stereotactic delivery of the virus and optic fibers into the right ACC of mice at 7–8 weeks of age. After 19–21 days, mice were habituated to a dummy optical patch cord (Doric Lenses Inc., MFP_100/125/900-0.22_2m_FC-ZF1.25 with flange) attached to a zirconia sleeve (Doric Lenses, SLEEVE_ZR_1.25) for ~15 min daily over 3–4 days while being handled with cotton gloves. Subsequently, mice underwent observational fear conditioning with photostimulation, followed by a contextual memory retrieval test 24 h later without optical cable attachment. Optogenetic stimulation of NpHR was achieved using a diode-pumped solid-state yellow laser (MGL-FN-561, 561 nm, Changchun New Industries Optoelectronics Technology Corp.), delivering continuous yellow light (0.9–1.8 mW) at the tip of a 200 μm optic fiber, with stimulation initiated 1 s prior to behavioral tasks.

Behavioral assays

Observational fear learning. Observational fear conditioning was performed by placing male mice (10–12 weeks old) individually in chambers divided by a transparent Plexiglas divider. After a 5 min habituation period, the demonstrator mouse received a 2 s foot shock (1 mA) every 10 s for 4 min. Observer mice were tested for contextual memory retrieval 24 h later by reintroducing them to the same chamber for 4 min. Freezing behavior was defined as the absence of movement for >1 s. Observer and demonstrator mice were neither siblings nor cage mates. Behavior was recorded using Freezeframe3 software (Coulbourn Instruments) and analyzed with FreezeView software (Coulbourn Instruments).

Contextual fear conditioning. For contextual fear conditioning, mice were placed in a fear conditioning chamber (Coulbourn Instruments) and allowed to explore for 5 min. They then received three 0.7 mA foot shocks (2 kHz pure tone) with 1-min intervals. Mice remained in the chamber for an additional 60 s before being returned to their home cages. Contextual fear memory was assessed 24 h later by placing mice back into the original chamber, while cued fear memory was tested in a novel chamber with the same auditory cue. Behavior was recorded and analyzed using Freeze Frame software.

Visual stimuli for looming stress. The experiment was controlled to have no sudden unexpected noise or visual cues. A looming stimulus (2 sec for expanding and 7 sec for pausing, 14 cm block-colored diameter) was delivered with a LED screen facing the arena from above. For the loss-of-function experiment, mice were placed in a cage with bedding, positioned under the same LED screen, and habituated for 20 min. When mice were in the center of the cage, the expanding looming stimulus was started. All trials were recorded by a USB camera (C922, Logitech) attached to a computer, and freezing behavior was analyzed using Adobe Premiere Pro software[80].

Reporting summary

Further information on research design is available in the Nature Portfolio Reporting Summary linked to this article.

Data availability

All data generated or analyzed during this study are included in this published article (and its supplementary information files). Source data are provided with this paper.

References

1. Olsson, A. & Phelps, E. A. Social learning of fear. *Nat. Neurosci.* **10**, 1095–1102 (2007).
2. Barrett, L. F., Mesquita, B., Ochsner, K. N. & Gross, J. J. The experience of emotion. *Annu. Rev. Psychol.* **58**, 373–403 (2007).
3. Keum, S. & Shin, H.-S. Neural basis of observational fear learning: a potential model of affective empathy. *Neuron* **104**, 78–86 (2019).
4. Debiec, J. & Olsson, A. Social fear learning: from animal models to human function. *Trends Cogn. Sci.* **21**, 546–555 (2017).
5. Burkett, J. P. et al. Oxytocin-dependent consolation behavior in rodents. *Science* **351**, 375–378 (2016).
6. Hernandez-Lallement, J. et al. Harm to others acts as a negative reinforcer in rats. *Curr. Biol.* **30**, 949–961.e7 (2020).
7. Jeon, D. et al. Observational fear learning involves affective pain system and Cav1.2 Ca2+ channels in ACC. *Nat. Neurosci.* **13**, 482–488 (2010).
8. Atsak, P. et al. Experience modulates vicarious freezing in rats: a model for empathy. *PLoS ONE* **6**, e21855 (2011).
9. Sanders, J., Mayford, M. & Jeste, D. Empathic fear responses in mice are triggered by recognition of a shared experience. *PLoS ONE* **8**, e74609 (2013).
10. Keum, S. et al. A missense variant at the Nrxn3 locus enhances empathy fear in the mouse. *Neuron* **98**, 588–601.e5 (2018).
11. Kim, B. S. et al. Differential regulation of observational fear and neural oscillations by serotonin and dopamine in the mouse anterior cingulate cortex. *Psychopharmacology* **231**, 4371–4381 (2014).
12. Pisansky, M. T., Hanson, L. R., Gottesman, I. I. & Gewirtz, J. C. Oxytocin enhances observational fear in mice. *Nat. Commun.* **8**, 2102 (2017).
13. Terranova, J. I. et al. Hippocampal-amygdala memory circuits govern experience-dependent observational fear. *Neuron* **110**, 1416–1431.e13 (2022).
14. Kim, S., Mátyás, F., Lee, S., Acsády, L. & Shin, H.-S. Lateralization of observational fear learning at the cortical but not thalamic level in mice. *Proc. Natl. Acad. Sci. Usa.* **109**, 15497–15501 (2012).
15. Kim, S.-W. et al. Hemispherically lateralized rhythmic oscillations in the cingulate-amygdala circuit drive affective empathy in mice. *Neuron* **111**, 418–429.e4 (2023).
16. Sara, S. J. The locus coeruleus and noradrenergic modulation of cognition. *Nat. Rev. Neurosci.* **10**, 211–223 (2009).
17. Sara, S. J. & Bouret, S. Orienting and reorienting: the locus coeruleus mediates cognition through arousal. *Neuron* **76**, 130–141 (2012).
18. Jordan, R. & Keller, G. B. The locus coeruleus broadcasts prediction errors across the cortex to promote sensorimotor plasticity. *eLife* **12**, RP85111 (2023).
19. Lee, T.-H. et al. Arousal increases neural gain via the locus coeruleus-norepinephrine system in younger adults but not in older adults. *Nat. Hum. Behav.* **2**, 356–366 (2018).
20. Maness, E. B. et al. Role of the locus coeruleus and basal forebrain in arousal and attention. *Brain Res. Bull.* **188**, 47–58 (2022).
21. Choucry, A., Ghandour, K. & Inokuchi, K. The locus coeruleus as a regulator of memory linking. *Neuron* **110**, 3227–3229 (2022).
22. Giustino, T. F., Ramanathan, K. R., Totty, M. S., Miles, O. W. & Maren, S. Locus coeruleus norepinephrine drives stress-induced increases in basolateral amygdala firing and impairs extinction learning. *J. Neurosci.* **40**, 907–916 (2020).
23. Giustino, T. F. & Maren, S. Noradrenergic modulation of fear conditioning and extinction. *Front. Behav. Neurosci.* **12**, 43 (2018).
24. Faber, E. S. L. et al. Modulation of SK channel trafficking by beta adrenoceptors enhances excitatory synaptic transmission and plasticity in the amygdala. *J. Neurosci. J. Soc. Neurosci.* **28**, 10803–10813 (2008).
25. Likhtik, E. & Johansen, J. P. Neuromodulation in circuits of aversive emotional learning. *Nat. Neurosci.* **22**, 1586–1597 (2019).
26. Hormigo, S. et al. The noradrenergic projection from the locus coeruleus to the cochlear root neurons in rats. *Brain Struct. Funct.* **220**, 1477–1496 (2015).

27. Lee, S.-B., Beak, S. K., Park, S. H., Waterhouse, B. D. & Lee, H. S. Collateral projection from the locus coeruleus to whisker-related sensory and motor brain regions of the rat. *J. Comp. Neurol.* **514**, 387–402 (2009).

28. Koga, K. et al. Ascending noradrenergic excitation from the locus coeruleus to the anterior cingulate cortex. *Mol. Brain* **13**, 49 (2020).

29. Hong, E.-H. & Choi, J.-S. Observational threat conditioning is induced by circa-strike activity burst but not freezing and requires visual attention. *Behav. Brain Res.* **353**, 161–167 (2018).

30. Soya, S. et al. Orexin receptor-1 in the locus coeruleus plays an important role in cue-dependent fear memory consolidation. *J. Neurosci.* **33**, 14549–14557 (2013).

31. Schwarz, L. A. et al. Viral-genetic tracing of the input–output organization of a central norepinephrine circuit. *Nature* **524**, 88–92 (2015).

32. Kim, J.-H. et al. Yin-and-yang bifurcation of opioidergic circuits for descending analgesia at the midbrain of the mouse. *Proc. Natl. Acad. Sci. USA.* **115**, 11078–11083 (2018).

33. Kang, S. J., Kim, J.-H., Kim, D.-I., Roberts, B. Z. & Han, S. A ponto-mesencephalic PACAPergic pathway underlying panic-like behavioral and somatic symptoms in mice. *Nat. Neurosci.* **27**, 90–101 (2024).

34. Robertson, S. D., Plummer, N. W. & Jensen, P. Uncovering diversity in the development of central noradrenergic neurons and their efferents. *Brain Res* **1641**, 234–244 (2016).

35. Uematsu, A., Tan, B. Z. & Johansen, J. P. Projection specificity in heterogeneous locus coeruleus cell populations: implications for learning and memory. *Learn. Mem.* **22**, 444–451 (2015).

36. McCall, J. G. et al. Locus coeruleus to basolateral amygdala noradrenergic projections promote anxiety-like behavior. *eLife* **6**, e18247 (2017).

37. Khalil, V. et al. Subcortico-amygdala pathway processes innate and learned threats. *eLife* **12**, e85459 (2023).

38. Bush, D. E. A., Caparosa, E. M., Gekker, A. & LeDoux, J. Beta-adrenergic receptors in the lateral nucleus of the amygdala contribute to the acquisition but not the consolidation of auditory fear conditioning. *Front. Behav. Neurosci.* **4**, 154 (2010).

39. Schiff, H. C. et al. β-adrenergic receptors regulate the acquisition and consolidation phases of aversive memory formation through distinct, temporally regulated signaling pathways. *Neuropsychopharmacology* **42**, 895–903 (2017).

40. Benarroch, E. E. Locus coeruleus. *Cell Tissue Res* **373**, 221–232 (2018).

41. Wu, D. et al. Persistent neuronal activity in anterior cingulate cortex correlates with sustained attention in rats regardless of sensory modality. *Sci. Rep.* **7**, 43101 (2017).

42. Newman, L. A. & McGaughy, J. Attentional effects of lesions to the anterior cingulate cortex: how prior reinforcement influences distractibility. *Behav. Neurosci.* **125**, 360–371 (2011).

43. Wilmot, J. H. et al. Phasic locus coeruleus activity enhances trace fear conditioning by increasing dopamine release in the hippocampus. *eLife* **12**, RP91465 (2024).

44. Ruggiero, R. N. et al. Neuromodulation of hippocampal-prefrontal cortical synaptic plasticity and functional connectivity: implications for neuropsychiatric disorders. *Front. Cell. Neurosci.* **15**, 732360 (2021).

45. Broncel, A., Bocian, R., Kłos-Wojtczak, P. & Konopacki, J. Effects of locus coeruleus activation and inactivation on hippocampal formation theta rhythm in anesthetized rats. *Brain Res. Bull.* **162**, 180–190 (2020).

46. Nuñez, A. & Buño, W. The theta rhythm of the hippocampus: from neuronal and circuit mechanisms to behavior. *Front. Cell. Neurosci.* https://doi.org/10.3389/fncel.2021.649262 (2021).

47. Lesting, J. et al. Patterns of coupled theta activity in amygdala-hippocampal-prefrontal cortical circuits during fear extinction. *PLoS ONE* **6**, e21714 (2011).

48. Hasselmo, M. E., Hay, J., Ilyn, M. & Gorchetchnikov, A. Neuromodulation, theta rhythm and rat spatial navigation. *Neural Netw* **15**, 689–707 (2002).

49. Chrastil, E. R. et al. Theta oscillations support active exploration in human spatial navigation. *NeuroImage* **262**, 119581 (2022).

50. Buzsáki, G. & Moser, E. I. Memory, navigation and theta rhythm in the hippocampal-entorhinal system. *Nat. Neurosci.* **16**, 130–138 (2013).

51. Spyropoulos, G., Bosman, C. A. & Fries, P. A theta rhythm in macaque visual cortex and its attentional modulation. *Proc. Natl. Acad. Sci. USA* **115**, E5614–E5623 (2018).

52. Buzsáki, G. Theta oscillations in the hippocampus. *Neuron* **33**, 325–340 (2002).

53. Seidenbecher, T., Laxmi, T. R., Stork, O. & Pape, H.-C. Amygdalar and hippocampal theta rhythm synchronization during fear memory retrieval. *Science* **301**, 846–850 (2003).

54. Li, S. The β-adrenergic hypothesis of synaptic and microglial impairment in Alzheimer's disease. *J. Neurochem.* **165**, 289–302 (2023).

55. Hertz, L., Lovatt, D., Goldman, S. A. & Nedergaard, M. Adrenoceptors in brain: cellular gene expression and effects on astrocytic metabolism and [Ca2+]i. *Neurochem. Int.* **57**, 411–420 (2010).

56. O'Dell, T. J., Connor, S. A., Guglietta, R. & Nguyen, P. V. β-Adrenergic receptor signaling and modulation of long-term potentiation in the mammalian hippocampus. *Learn. Mem.* **22**, 461–471 (2015).

57. Qian, H. et al. Phosphorylation of Ser1928 mediates the enhanced activity of the L-type Ca2+ channel Cav1.2 by the β2-adrenergic receptor in neurons. *Sci. Signal.* **10**, eaaf9659 (2017).

58. Patriarchi, T. et al. Phosphorylation of Cav1.2 on S1928 uncouples the L-type Ca2+ channel from the β2 adrenergic receptor. *EMBO J.* **35**, 1330–1345 (2016).

59. Liu, Y., Rodenkirch, C., Moskowitz, N., Schriver, B. & Wang, Q. Dynamic lateralization of pupil dilation evoked by locus coeruleus activation results from sympathetic not parasympathetic contributions. *Cell Rep.* **20**, 3099–3112 (2017).

60. Làdavas, E. & Bertini, C. Right hemisphere dominance for unconscious emotionally salient stimuli. *Brain Sci.* **11**, 823 (2021).

61. Ross, J. A. & Van Bockstaele, E. J. The locus coeruleus- norepinephrine system in stress and arousal: unraveling historical, current, and future perspectives. *Front. Psychiatry* https://doi.org/10.3389/fpsyt.2020.601519 (2021).

62. Van Bockstaele, E. J., Colago, E. E. O. & Valentino, R. J. Amygdaloid corticotropin-releasing factor targets locus coeruleus dendrites: substrate for the co-ordination of emotional and cognitive Limbs of the stress response. *J. Neuroendocrinol.* **10**, 743–758 (1998).

63. Simpson, K. L. et al. Lateralization and functional organization of the locus coeruleus projection to the trigeminal somatosensory pathway in rat. *J. Comp. Neurol.* **385**, 135–147 (1997).

64. Goode, T. D., Ressler, R. L., Acca, G. M., Miles, O. W. & Maren, S. Bed nucleus of the stria terminalis regulates fear to unpredictable threat signals. *eLife* **8**, e46525 (2019).

65. van de Poll, Y., Cras, Y. & Ellender, T. J. The neurophysiological basis of stress and anxiety - comparing neuronal diversity in the bed nucleus of the stria terminalis (BNST) across species. *Front. Cell. Neurosci.* https://doi.org/10.3389/fncel.2023.1225758 (2023).

66. Pitts, M. W., Todorovic, C., Blank, T. & Takahashi, L. K. The central nucleus of the amygdala and corticotropin-releasing factor: insights into contextual fear memory. *J. Neurosci.* **29**, 7379–7388 (2009).

67. Gilpin, N. W., Herman, M. A. & Roberto, M. The central amygdala as an integrative hub for anxiety and alcohol use disorders. *Biol. Psychiatry* **77**, 859–869 (2015).

68. Mazzone, C. M. et al. Acute engagement of Gq-mediated signaling in the bed nucleus of the stria terminalis induces anxiety-like behavior. *Mol. Psychiatry* **23**, 143–153 (2018).

69. Straube, T., Mentzel, H.-J. & Miltner, W. H. R. Waiting for spiders: brain activation during anticipatory anxiety in spider phobics. *NeuroImage* **37**, 1427–1436 (2007).

70. Mobbs, D. et al. Neural activity associated with monitoring the oscillating threat value of a tarantula. *Proc. Natl. Acad. Sci. USA* **107**, 20582–20586 (2010).

71. Davis, M., Walker, D. L., Miles, L. & Grillon, C. Phasic vs sustained fear in rats and humans: role of the extended amygdala in fear vs anxiety. *Neuropsychopharmacology* **35**, 105–135 (2010).

72. Hammack, S. E., Todd, T. P., Kocho-Schellenberg, M. & Bouton, M. E. Role of the bed nucleus of the stria terminalis in the acquisition of contextual fear at long or short context-shock intervals. *Behav. Neurosci.* **129**, 673–678 (2015).

73. Lee, Y. & Davis, M. Role of the hippocampus, the bed nucleus of the stria terminalis, and the amygdala in the excitatory effect of corticotropin-releasing hormone on the acoustic startle reflex. *J. Neurosci.* **17**, 6434–6446 (1997).

74. Orion, P., Keifer, J., Hurt, R. C., Ressler, K. J. & Marvar, P. J. The physiology of fear: reconceptualizing the role of the central amygdala in fear learning. *Physiology* **30**, 389 (2015).

75. Maren, S. Unrelenting fear under stress: neural circuits and mechanisms for the immediate extinction deficit. *Front. Syst. Neurosci.* https://doi.org/10.3389/fnsys.2022.888461 (2022).

76. Yan, C.-Q. et al. Abnormal functional connectivity of anterior cingulate cortex in patients with primary insomnia: a resting-state functional magnetic resonance imaging study. *Front. Aging Neurosci.* **10**, 167 (2018).

77. Muzur, A., Pace-Schott, E. F. & Hobson, J. A. The prefrontal cortex in sleep. *Trends Cogn. Sci.* **6**, 475–481 (2002).

78. Nofzinger, E. A. et al. Functional neuroimaging evidence for hyperarousal in insomnia. *Am. J. Psychiatry* **161**, 2126–2128 (2004).

79. Sanford, L. D., Parris, B. & Tang, X. GABAergic regulation of the central nucleus of the amygdala: implications for sleep control. *Brain Res.* **956**, 276–284 (2002).

80. Li, L. et al. Stress accelerates defensive responses to looming in mice and involves a locus coeruleus-superior colliculus projection. *Curr. Biol.* **28**, 859–871.e5 (2018).

Acknowledgements

Author contributions

J.-H.Kim. and H.-S.Shin. conceived the project and designed all experiments. J.-H.Kim. performed all behavioral assays, surgeries, photometry assays, tracing, and optogenetic experiments. J.-H.Kim. and D.-E.Choi. performed the histology experiments. J.-H.Kim. and H.-S.Shin. wrote the manuscript.

Competing interests

The authors declare no competing interests.

Additional information

Supplementary information The online version contains supplementary material available at https://doi.org/10.1038/s41467-025-57701-0.

Correspondence and requests for materials should be addressed to Hee-Sup Shin.

Peer review information *Nature Communications* thanks Tao Chen and Takashi Kitamura for their contribution to the peer review of this work. A peer review file is available.

Reprints and permissions information is available at http://www.nature.com/reprints

Publisher's note Springer Nature remains neutral with regard to jurisdictional claims in published maps and institutional affiliations.